

# True-Time-Delay Arrays for Fast Beam Training in Wideband Millimeter-Wave Systems

Veljko Boljanovic, *Student Member, IEEE*, Han Yan, *Student Member, IEEE*,  
 Chung-Ching Lin, *Student Member, IEEE*, Soumen Mohapatra, *Student Member, IEEE*,  
 Deukhyoun Heo, *Senior Member, IEEE*, Subhanshu Gupta, *Senior Member, IEEE*,  
 and Danijela Cabric, *Senior Member, IEEE*

**Abstract**—The best beam steering directions are estimated through beam training, which is one of the most important and challenging tasks in millimeter-wave and sub-terahertz communications. Novel array architectures and signal processing techniques are required to avoid prohibitive beam training overhead associated with large antenna arrays and narrow beams. In this work, we leverage recent developments in true-time-delay (TTD) arrays with large delay-bandwidth products to accelerate beam training using frequency-dependent probing beams. We propose and study two TTD architecture candidates, including analog and hybrid analog-digital arrays, that can facilitate beam training with only one wideband pilot. We also propose a suitable algorithm that requires a single pilot to achieve high-accuracy estimation of angle of arrival. The proposed array architectures are compared in terms of beam training requirements and performance, robustness to practical hardware impairments, and power consumption. The findings suggest that the analog and hybrid TTD arrays achieve a sub-degree beam alignment precision with 66% and 25% lower power consumption than a fully digital array, respectively. Our results yield important design trade-offs among the basic system parameters, power consumption, and accuracy of angle of arrival estimation in fast TTD beam training.

**Index Terms**—True-time-delay array, array architecture, beam training, millimeter-wave communication, wideband systems

## I. INTRODUCTION

**A**BUNDANT spectrum at millimeter-wave (mmW) frequencies is seen as the key resource for providing high data rates in the fifth generation of cellular systems [1]. However, the use of mmW communication bands comes at the cost of less favorable propagation conditions [2]. Both the base station (BS) and user equipment (UE) are required to use large antenna arrays to achieve high beamforming (BF) gain and compensate for severe propagation loss. Beam pointing directions are estimated through *beam training*, a procedure that identifies the angle of arrival (AoA) and angle

of departure (AoD) of the dominant propagation path in the wireless channel. Apart from aligning the beams for data communication, knowledge of the AoA and AoD is of utmost importance for other applications in practical mmW systems, including interference nulling and localization [3].

The existing mmW systems utilize analog array architecture with a single transceiver radio frequency (RF)-chain at both the BS and UE due to its power efficiency. Such arrays are referred to as phased arrays since they use adjustable phase shifters to allow coherent signal steering/combining in a desired direction. The existing beam training schemes with phased arrays include various types of extensive beam sweeping, where beams with different pointing directions are synthesised to probe the channel sequentially in order to find the AoD and AoA [4]–[7]. The required number of probing beams linearly scales with the number of antenna elements in the array, which directly translates into beam training overhead and latency. Hence, conventionally used beam sweeping faces scalability challenge in higher mmW frequency bands, where more antenna elements will be used to achieve the required BF gain.

Previous work that addresses the beam training problem can be divided into two categories. The first category intends to reduce the required number of probing beams. Specifically, the number scales logarithmically with the array size when advanced signal processing techniques that exploit the sparsity of mmW channel are used [8]–[10]. Further, various side-information, e.g., location information and out-of-band measurements [11], can also be used to reduce the required number of probing beams. The second category aims to enhance the simultaneous channel probing capability by using advanced hardware design [12]–[19]. These approaches are more robust when the channel sparsity and side information are not available. Fully digital array architectures, with a dedicated RF-chain per each antenna element, offer the highest flexibility and capability of channel probing. From the signal processing perspective, signals from all antenna branches can be steered/combined to simultaneously probe all angular directions for fast AoD/AoA estimation [12]–[14]. Fully-connected or sub-band based hybrid arrays are another way to enhance simultaneous probing of the channel [15]–[17]. They can probe multiple directions simultaneously and the flexibility increases linearly with the number of RF-chains that control phase shifter based analog front-end [12]. The probing capability of hybrid arrays can be further enhanced by associating probing

This work was supported in part by NSF under grants 1718742, 1705026, and 1944688. This work was also supported in part by the ComSenTer and CONIX Research Centers, two of six centers in JUMP, a Semiconductor Research Corporation (SRC) program sponsored by DARPA.

Veljko Boljanovic, Han Yan, and Danijela Cabric are with the Department of Electrical and Computer Engineering, University of California, Los Angeles, Los Angeles, CA 90095 USA (e-mail: vboljanovic@ucla.edu, yhaddint@ucla.edu, danijela@ee.ucla.edu).

Chung-Ching Lin, Soumen Mohapatra, Deukhyoun Heo, and Subhanshu Gupta are with the School of Electrical Engineering and Computer Science, Washington State University, Pullman, WA 99164 USA (e-mail: chung-ching.lin@wsu.edu, soumen.mohapatra@wsu.edu, dheo@wsu.edu, sgupta@eecs.wsu.edu).

beams with different frequencies using spatio-spectral BF [15]. Leaky wave antenna (LWA) can scan all angular directions simultaneously by using different frequency resources since the pointing directions of the beams are frequency-dependent [18], [19]. However, the existing LWA technique requires access to THz spectrum for adequate frequency dispersive beam steering.

TTD arrays are another appealing, yet insufficiently investigated alternative for fast mmW beam training. Due to time delaying of the signal in each antenna branch, TTD arrays have frequency-dependent probing beams, which can be exploited to enhance the channel probing capability. Further, the frequency-dependent beams can be fully controlled by adjusting the delay introduced in TTD circuits [20]. Early implementations relied on delay lines in all antenna branches [21], but this approach suffered from low scalability in terms of required area and power efficiency when the array size becomes large. Further, limited delay range at RF is insufficient to achieve frequency dispersive beam training as proposed in this work. Recent advancement in TTD arrays with baseband delay elements and large delay range-to-resolution ratios [22], [23], improved the scalability and thus enabled the realization of fast beam training schemes with large arrays.

In this paper, we extend our previous work [24] and present the design of baseband TTD array architectures for mmW beam training. To the best of our knowledge, this is the first work that comprehensively study the system and circuit aspects of TTD based mmW beam training with dispersive channel probing. The key contributions are summarized as follows:

- We propose two TTD architecture candidates with baseband delay elements for fast beam training: 1) analog TTD architecture, where signal delaying is done in analog baseband domain; 2) hybrid analog-digital TTD architecture, where signal delaying is done both in analog and digital domains.
- We propose a power measurement based beam training scheme for TTD arrays that requires only one training pilot. In particular, we design frequency-dependent probing beams robust to frequency-selective mmW channels and a digital signal processing (DSP) algorithm for high-accuracy angle estimation. We numerically evaluate the performance of the proposed algorithm in a practical multipath fading channel.
- We study the required TTD hardware specifications of both array architectures and we explain how hardware constraints affect the beam training performance. We also quantitatively study the beam training performance under practical hardware impairments of TTD array circuits, including phase errors, delay compensation errors, and analog-to-digital converter (ADC) quantization errors. We include the performance of a fully digital array as the benchmark.
- We model and estimate the power consumption of the proposed TTD array architectures in the beam training framework. We investigate how power consumption scales with the key system parameters, including the bandwidth and array size, which provides an insight

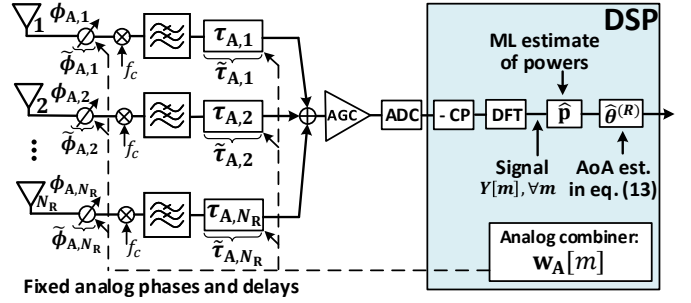


Fig. 1. Architecture of analog TTD array with uniform delay spacing  $\Delta\tau$  and phase spacing  $\Delta\phi$  between antennas. The design of combiners and DSP algorithm is explained in Section III-B.

into the beam training design in future mmW/sub-THz systems. Power consumption of the fully digital array is included as the benchmark.

The rest of the paper is organized as follows. In Section II, we introduce the two TTD architectures and benchmark fully digital array. Section III introduces a wideband system model and it describes the beam training codebook and DSP algorithm design. In Section IV, we explain the baseband implementation of TTD elements and compare the considered architectures in terms of the beam training performance under practical hardware impairments. Power consumption of all three considered architectures is modeled and evaluated in Section V. Section VI concludes the paper.

## II. TTD ARRAY ARCHITECTURES FOR BEAM TRAINING

The realization and performance of TTD beam training schemes heavily depends on the underlying TTD hardware. The design of a fast high performance beam training scheme imposes a challenging delay range requirement on TTD circuits, which raises the question of a *beam-training-efficient* TTD array architecture. In this work, the efficiency depends the number of pilots used in beam training, angle estimation accuracy, and array power consumption. To address this question, we propose and extensively compare two uniform linear array architectures with baseband TTD elements, including analog and hybrid analog-digital arrays. We include a fully digital array architecture in the comparison as the benchmark due to its known flexibility and high beam training performance. All three considered array architectures are described in the reminder of this section.

An analog uniform linear TTD array with a single RF-chain and  $N_R$  antennas is presented in Fig. 1. The  $n$ -th antenna branch has an analog phase shifter with the phase tap  $\phi_{A,n} = (n-1)\Delta\phi$  and an analog baseband TTD element with the delay tap  $\tau_{A,n} = (n-1)\Delta\tau$ , where  $\Delta\phi$  and  $\Delta\tau$  represent the phase and delay spacing between neighboring branches, respectively. Due to the hardware errors in practical phase shifters and TTD elements, the phase and delay taps can be distorted. In all antenna branches, we model the time-invariant distorted taps as independent zero-mean Gaussian random variables  $\check{\phi}_{A,n} \sim \mathcal{N}(\phi_{A,n}, \sigma_P^2)$  and  $\check{\tau}_{A,n} \sim \mathcal{N}(\tau_{A,n}, \sigma_T^2)$ , respectively. For a specific delay spacing  $\Delta\tau$ , TTD frequency-dependent antenna weight vector (AWV) results in a fixed beam training codebook, where different

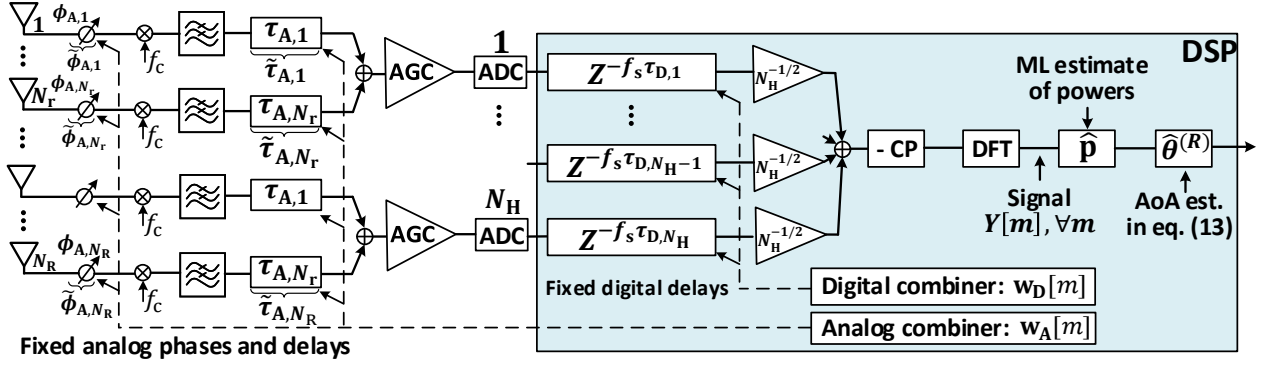


Fig. 2. Architecture of hybrid analog-digital TTD array with uniform delay spacing  $\Delta\tau$  and phase spacing  $\Delta\phi$  between antennas. The design of combiners and DSP algorithm is explained in Section III-B.

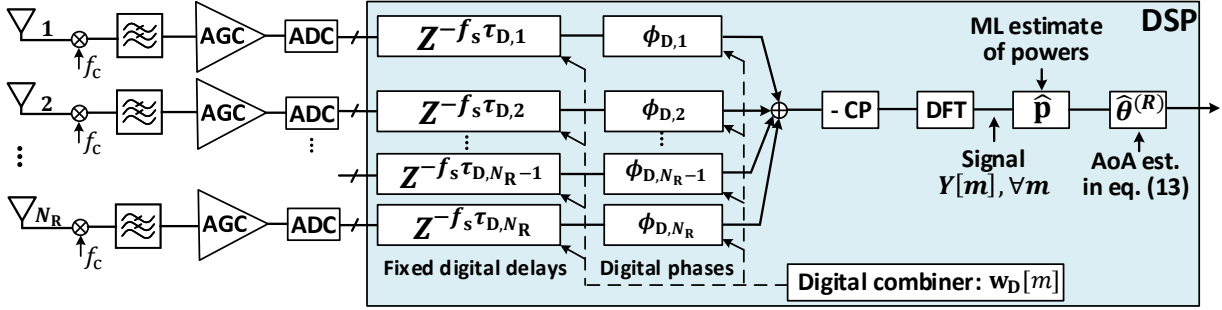


Fig. 3. Architecture of the benchmark fully digital array that emulates a TTD architecture by introducing digital delays. The design of combiners and DSP algorithm is explained in Section III-B.

frequency components of the signal are hard-coded in different angular directions. The frequency-flat phase shifters increase the flexibility by enabling codebook rotations and different frequency-to-angle mapping. The maximum delay in the  $N_R$ -th antenna branch is  $\tau_{A,N_R} = (N_R - 1)\Delta\tau$ , which becomes an implementation bottleneck for large antenna arrays. The state-of-the-art TTD delay range is in the order of 15 ns [22], which can be insufficient for wideband beam training with a moderate number of antenna elements  $N_R$ , e.g.,  $N_R = 32$ , as we previously discussed in [24].

To alleviate the delay range requirement and improve the scalability of analog TTD arrays, we introduce a hybrid analog-digital architecture with  $N_H$  sub-arrays, each controlled by one distinct RF-chain, as illustrated in Fig. 2. The hybrid array uses a combination of analog and digital signal delaying, where first all the sub-arrays of  $N_r$  antennas introduce the same delays  $\tau_{A,n'} = (n' - 1)\Delta\tau$ ,  $n' = 1, \dots, N_r$ , in the analog domain. The relative delay difference among antennas is compensated in the digital domain by introducing the fixed digital taps  $\tau_{D,h} = (h - 1)N_r\Delta\tau$ ,  $h = 1, \dots, N_H$ , i.e., digital delays  $f_s\tau_{D,h}$ , where  $f_s$  is the sampling frequency. As in the analog TTD array, the distorted phase taps  $\phi_{A,n}$ ,  $n = 1, \dots, N_R$ , and delay taps  $\tau_{A,n}$ ,  $n = 1, \dots, N_R$ , are modeled as independent Gaussian random variables.

A fully digital array, used as the benchmark, is illustrated in Fig. 3. The digital array can emulate a TTD array through DSP by using the fixed digital taps  $\tau_{D,n} = (n - 1)\Delta\tau$ ,  $n = 1, \dots, N_R$ , i.e., digital delays  $f_s\tau_{D,n}$  in the corresponding antenna branches. The ability to control the digital phases  $\phi_{D,n}$ ,  $n = 1, \dots, N_R$ , in DSP, allows the signal frequency components to be independently steered/combined in any

angular direction, which provides high flexibility in the beam training design. The digital array does not have the phase shifters and TTD elements before the ADCs, thus we assume it is insensitive to hardware errors. However, each antenna element has a dedicated RF-chain, which significantly affects the array power efficiency, as discussed later in Section V.

In the next section, we explain how  $\Delta\tau$  and  $\Delta\phi$  are set up in all three architecture to obtain a beam training codebook robust to frequency-selective channels. We also introduce a DSP algorithm that exploits this codebook. Based on the designed  $\Delta\tau$ , Section IV discusses the requirements in TTD hardware implementation and impact of hardware impairments on the beam training performance. Accounting for the designed  $\Delta\tau$  and proposed baseband TTD implementation, we compare the three architectures in terms of power consumption in Section V.

### III. TTD BEAM TRAINING ALGORITHM DESIGN

In this section, we describe a DSP algorithm which achieves a high angle estimation accuracy using only one pilot symbol in a clustered frequency-selective multipath channel. An example of such channel with one strong and one weak cluster, as seen by the receiver, is provided in Fig. 4(a). Conventional phased arrays cannot estimate the AoA of the dominant cluster with one training pilot, and thus they require beam sweeping, as illustrated in Fig. 4(b). On the other hand, TTD arrays are capable of estimating the AoA fast, but the corresponding DSP algorithm must include the design of a suitable TTD beam training codebook.

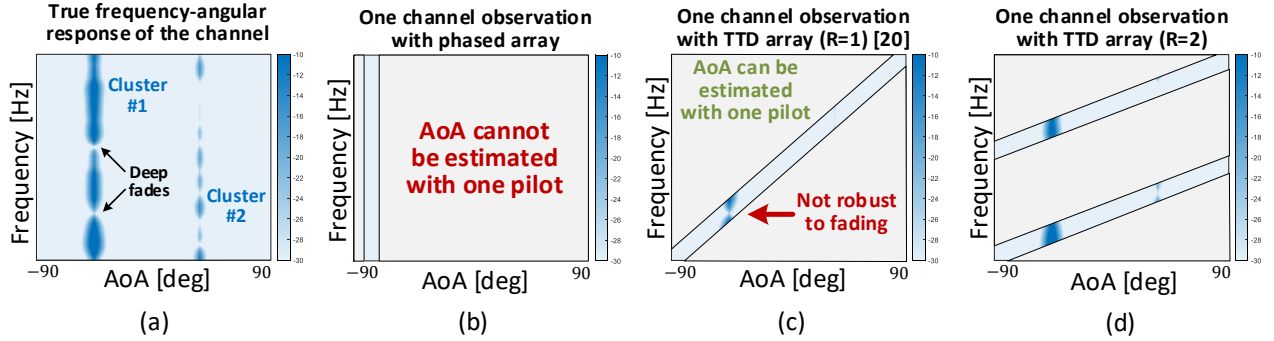


Fig. 4. Beam training in clustered frequency-selective multipath channel: (a) An example of frequency-selective channel with two multipath clusters. Frequency-selectivity comes from intra- and inter-cluster delay spreads. (b) Channel observation of a phased array when only one pilot is used. Beam sweeping is necessary to cover all angles in the range  $(-\pi/2, \pi/2)$ . (c) Channel observation of a TTD array when only one pilot is used. Frequency components (subcarriers) are mapped into different angles to simultaneously probe the range  $(-\pi/2, \pi/2)$ . The angle estimation may fail in frequency-selective channels. (d) Enhanced TTD codebook with frequency diversity order  $R = 2$ .

### A. System Model

We consider downlink beam training between the BS and UE, where the cyclic prefix (CP) based orthogonal frequency-division multiplexing (OFDM) waveform is used as a training pilot. The carrier frequency, bandwidth, and number of subcarriers are denoted as  $f_c$ , BW, and  $M_{\text{tot}}$ , respectively. The power-normalized training pilot uses  $M$  subcarriers from the predefined set  $\mathcal{M}$ , all loaded with the same binary phase shift keying modulated symbol. Both the BS and UE have half-wavelength spaced uniform linear arrays with  $N_T$  and  $N_R$  antennas, respectively. We assume that AoD at the BS has already been estimated so that BS uses a fixed frequency-flat beam defined by a precoder vector  $\mathbf{v} \in \mathbb{C}^{N_T}$ . The UE is equipped with a TTD array and it performs beam training to estimate AoA  $\hat{\theta}^{(R)}$ . Thus, the received signal  $Y[m]$  at the  $m$ -th subcarrier is

$$Y[m] = \mathbf{w}^H[m] \mathbf{H}[k] \mathbf{v} + \mathbf{w}^H[m] \mathbf{n}[m], \quad m \in \mathcal{M}, \quad (1)$$

where  $\mathbf{H}[k] \in \mathbb{C}^{N_R \times N_T}$  is the channel matrix of the  $k$ -th out of  $K_c$  sub-bands in a frequency-selective channel and  $\mathbf{n} \sim \mathcal{CN}(0, \sigma_n^2 \mathbf{I}_{N_R})$  is white Gaussian noise. Each sub-band contains multiple adjacent sub-carriers, and the relationship between the sub-band index  $k$  and subcarrier index  $m$  is given as  $k = \lceil (mK_c)/M_{\text{tot}} \rceil$ , where  $\lceil x \rceil$  rounds  $x$  to the nearest greater integer. We assume that all subcarriers within the same frequency sub-band  $k$  experience the same channel  $\mathbf{H}[k]$ . The TTD combiner  $\mathbf{w}[m] \in \mathbb{C}^{N_R}$  of the  $m$ -th subcarrier can be decomposed as a Hadamard product  $\mathbf{w}[m] = \mathbf{w}_A[m] \odot \mathbf{w}_D[m]$ , where the analog combiner  $\mathbf{w}_A[m] \in \mathbb{C}^{N_R}$  and digital combiner  $\mathbf{w}_D[m] \in \mathbb{C}^{N_R}$  depend on the underlying TTD array architecture. In an analog TTD array,  $\mathbf{w}_D[m] = \mathbf{1}_{N_R}$  since both the phases  $\phi_{A,n}$ ,  $\forall n$ , and delays  $\tau_{A,n}$ ,  $\forall n$ , are introduced in the analog domain. Similarly,  $\mathbf{w}_A[m] = \mathbf{1}_{N_R}$  with a fully digital array, as it is insensitive to hardware impairments and the phases  $\phi_{D,n}$ ,  $\forall n$ , and delays  $\tau_{D,n}$ ,  $\forall n$ , are applied in the digital domain. In general, the  $n$ -th elements of  $\mathbf{w}_A[m]$  and  $\mathbf{w}_D[m]$  are

$$[\mathbf{w}_A[m]]_n = \exp \left[ -j \left( 2\pi (f_m - f_c) \tilde{\tau}_{A,n} + \tilde{\phi}_{A,n} \right) \right] \quad (2)$$

$$[\mathbf{w}_D[m]]_n = \exp \left[ -j \left( 2\pi (f_m - f_c) \tau_{D,n} + \phi_{D,n} \right) \right] \quad (3)$$

where  $f_m = f_c - \text{BW}/2 + (m-1)\text{BW}/(M_{\text{tot}}-1)$ .

The expressions (2) and (3) indicate that the beam pointing direction depends on the subcarrier frequency, phases, and delays. With a proper configuration of the phase and delay taps in the analog and/or digital domain, it is possible to set up a codebook of combiners that covers all angular directions, as we discuss in the next subsection.

### B. DSP Algorithm for Beam Training

In this subsection, we first present the design of a robust codebook and then describe a DSP algorithm for TTD arrays [24] that achieves a high resolution in AoA estimation.

In [20], we have demonstrated that  $D$  spatial directions in the angular range  $(-\pi/2, \pi/2)$  can be sounded with a single OFDM symbol by mapping one subcarrier per direction, as illustrated in Fig. 4(c). We have shown that this can be achieved with an analog TTD array by setting the delay spacing to be  $\Delta\tau = 1/\text{BW}$ . The resulting codebook is, however, sensitive to frequency-selective channels since certain subcarriers can experience deep fades and thus miss to detect the incoming signal. The codebook can be enhanced by increasing its frequency diversity order  $R$ , i.e., by mapping  $R$  distinct subcarriers in each probed direction [24]. The benefit of the enhanced codebook is illustrated in Fig. 4(d) for  $R = 2$ , where two subcarriers detect the dominant cluster. To increase the diversity, we define  $D$  distinct sets  $\mathcal{M}_d$ ,  $1 \leq d \leq D$ , of  $R$  subcarriers, where each set is associated with a different direction  $d$ ,  $1 \leq d \leq D$ . Mathematically, the  $R$  subcarriers from the set  $\mathcal{M}_d$  have the same combiner  $\mathbf{f}_d$ , i.e.,  $\mathbf{w}[m] = \mathbf{f}_d$ ,  $\forall m \in \mathcal{M}_d$ , where the  $n$ -th element of  $\mathbf{f}_d$  is defined as

$$[\mathbf{f}_d]_n = \exp[-j2\pi(n-1)(d-1-D/2)/D], \quad d \leq D. \quad (4)$$

The subcarriers in  $\mathcal{M}_d$ ,  $\forall d$ , however, should experience different channels, and thus we choose them uniformly across the bandwidth with the step size larger or equal than the coherence bandwidth (channel sub-band size). This codebook can be created for an analog TTD array by setting the  $n$ -th phase and delay taps as follows

$$\phi_{A,n} = (n-1)[\text{sgn}(\psi)\pi - \psi] \quad (5)$$

$$\tau_{A,n} = (n-1)R/\text{BW}, \quad (6)$$

where  $\psi = \text{mod}(2\pi R(f_c - \text{BW}/2)/\text{BW} + \pi, 2\pi) - \pi$ .  $\text{sgn}()$  and  $\text{mod}()$  are the sign and modulo operators, respectively.

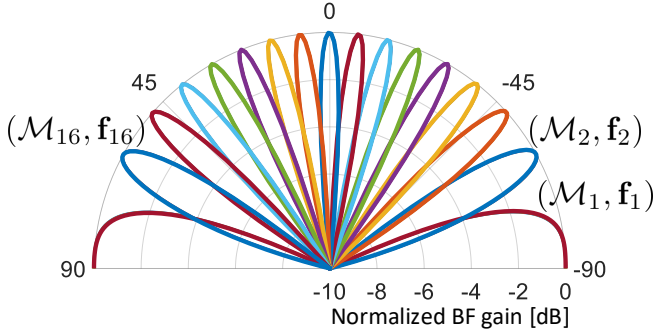


Fig. 5. An example of robust TTD codebook for  $N_R = 16$ ,  $D = 16$ , and  $R = 4$ . All  $D = 16$  directions are probed simultaneously. Direction  $d$ ,  $1 \leq d \leq D$ , is associated with set of subcarriers  $\mathcal{M}_d$  and combiner  $\mathbf{f}_d$ .

The phase taps in (5) ensure that the first set of subcarriers  $\mathcal{M}_1$  is mapped into the first probed angle  $(-\pi/2)$ . An example of the resulting codebook with  $N_R = 16$ ,  $D = 16$ , and  $R = 4$  is provided in Fig. 5. Note that the same enhanced codebook can be created for the hybrid TTD or fully digital array without the need to implement a fractional ADC sampling since  $\Delta\tau$  is proportional to the Nyquist sampling period, i.e.,  $\Delta\tau = R/\text{BW}$ . Analog and digital delay taps of the hybrid array introduced in Section II, can be expressed with respect to the indices of all antenna elements in the array  $n = 1, \dots, N_R$ , as  $\tau_{A,n} = (n - 1 - \lfloor (n - 1)/N_r \rfloor N_r) \Delta\tau$ , and  $\tau_{D,n} = \lfloor (n - 1)/N_r \rfloor N_r \Delta\tau$ , respectively. The operator  $\lfloor x \rfloor$  rounds  $x$  to the nearest lower integer. Thus, the hybrid TTD array can create the enhanced codebook by setting the  $n$ -th taps of its analog and digital combiners in the following way

$$\phi_{A,n} = (n - 1)[\text{sgn}(\psi)\pi - \psi], \quad (7)$$

$$\tau_{A,n} = (n - 1 - \lfloor (n - 1)/N_r \rfloor N_r) R/\text{BW}, \quad (8)$$

$$\tau_{D,n} = \lfloor (n - 1)/N_r \rfloor N_r R/\text{BW}, \quad (9)$$

where  $\psi$  is defined as earlier. The result in (9) suggests that the  $h$ -th sub-array needs to introduce a digital delay of  $2(h - 1)N_r R$  time samples, assuming the Nyquist sampling frequency  $f_s = 2\text{BW}$ . The considered hybrid array in Fig. 2 does not apply the phase changes in the digital domain. The digital array can create the enhanced codebook by using the following digital taps

$$\phi_{D,n} = (n - 1)\Delta\phi, \quad \Delta\phi \in \mathbb{R} \quad (10)$$

$$\tau_{D,n} = (n - 1)R/\text{BW}. \quad (11)$$

The phase tap in (10) implies that the digital array can leverage the DSP to introduce any number of phase spacings  $\Delta\phi$ . With  $f_s = 2\text{BW}$ , the  $n$ -th antenna branch will introduce the digital delay of  $2(n - 1)R$  time samples according to (11).

The phase and delay taps required for the design of a robust codebook are summarized in Table I for all three arrays.

TABLE I  
PHASE AND DELAY TAP SETTINGS FOR ROBUST CODEBOOK DESIGN

Array arch.	$\mathbf{w}[m]$	$\phi_{A,n}$	$\tau_{A,n}$	$\phi_{D,n}$	$\tau_{D,n}$
Analog TTD	$\mathbf{w}_A[m]$	(5)	(6)	N/A	N/A
Hybrid TTD	$\mathbf{w}_A[m] \odot \mathbf{w}_D[m]$	(7)	(8)	N/A	(9)
Digital	$\mathbf{w}_D[m]$	N/A	N/A	(10)	(11)

We note that the analog and hybrid TTD architectures have the same limited flexibility of receive combining in beam

training. Namely, once their corresponding analog combiners  $\mathbf{w}_A[m]$ ,  $m \in \mathcal{M}$ , and digital combiners  $\mathbf{w}_D[m]$ ,  $m \in \mathcal{M}$  are set up, they cannot be further changed or manipulated in DSP. In both architectures, this happens because the signals from different antenna branches are completely or partially combined before passing through ADCs. Thus, the inability to rotate the combiners limits the number of sounded directions to  $D$  in both arrays. The diversity order  $R$  is also limited, but not necessarily the same in both arrays, as discussed later in the paper. On the other hand, the digital array can exploit digitized signals in all antenna branches and combine them from many different directions in DSP by changing the phases  $\phi_{D,n}$ ,  $\forall n$ . Different phases  $\phi_{D,n}$  introduces angular shifts of the entire codebook, and enable scanning more angles and/or higher diversity.

We use the designed beam training codebook to develop a non-coherent power-based DSP angle estimation algorithm. Non-coherent algorithms are preferred in mmW beam training as they avoid complex joint synchronization and beam training receiver processing.

Since the subcarriers from  $\mathcal{M}_d$ ,  $\forall d$ , experience different channels, we can consider the received signal in all  $D$  probed directions as random. In a clustered multipath channel, the vector of expected powers in  $D$  directions  $\mathbf{p} = [p_1, p_2, \dots, p_D]^T$  can be expressed as

$$\mathbf{p} = \mathbf{B}\mathbf{g} + N_R\sigma_N^2\mathbf{1}, \quad (12)$$

where  $\mathbf{B} \in \mathbb{R}^{D \times Q}$  is a known dictionary obtained by generalizing the UE BF gains in  $Q$  angles  $\xi_q$ ,  $q = 1, \dots, Q$ , for all  $D$  combiners. The  $(d, q)$ -th element of  $\mathbf{B}$  is defined as  $[\mathbf{B}]_{d,q} = |\mathbf{f}_d^H \mathbf{a}_R(\xi_q)|^2$ , where  $\mathbf{a}_T(\xi_q)$  is the receive spatial response with elements  $[\mathbf{a}_R(\xi_q)]_n = N_R^{-1/2} \exp(-j(n - 1)\pi \sin(\xi_q))$ ,  $n = 1, \dots, N_R$ . The vector  $\mathbf{g} \in \mathbb{R}^Q$  has only one non-zero element. For a detailed derivation of (12), please refer to Appendix A.

During beam training, the estimates of  $p_d$ ,  $\forall d$ , are obtained by averaging out the powers of all subcarriers from the corresponding set  $\mathcal{M}_d$ ,  $\forall d$  [24]. In fact, it can be shown that the sample mean is the maximum likelihood (ML) estimator of  $p_d$ ,  $\forall d$ . The vector of power estimates is denoted as  $\hat{\mathbf{p}}$ , which approximate  $\mathbf{p}$  in (12). Based on the power measurement model in (12), AoA estimation can be solved based on the ML criterion using simple linear algebra operations. The AoA  $\theta^{(R)}$  estimate is obtained by finding the index of the column in  $\mathbf{B}$  which has the highest correlation with  $\hat{\mathbf{p}}$ , which is mathematically expressed as

$$\hat{\theta}^{(R)} = \xi_{q^*}, \quad \text{where } q^* = \underset{q}{\text{argmax}} \frac{\hat{\mathbf{p}}^T [\mathbf{B}]_{:,q}}{\|[\mathbf{B}]_{:,q}\|}. \quad (13)$$

The proposed algorithm can achieve high AoA estimation accuracy by increasing  $Q$ , i.e., the number of the columns in the dictionary matrix  $\mathbf{B}$ . Although this increases the DSP complexity, the proposed beam training scheme can still be performed with a single OFDM symbol. For the rest of this paper, we use root mean square error (RMSE) of AoA estimation and power consumption as main metrics for the comparison of the proposed TTD architectures. The AoA RMSE closely describes the beam training performance and it can be directly converted to an alternative metric in other

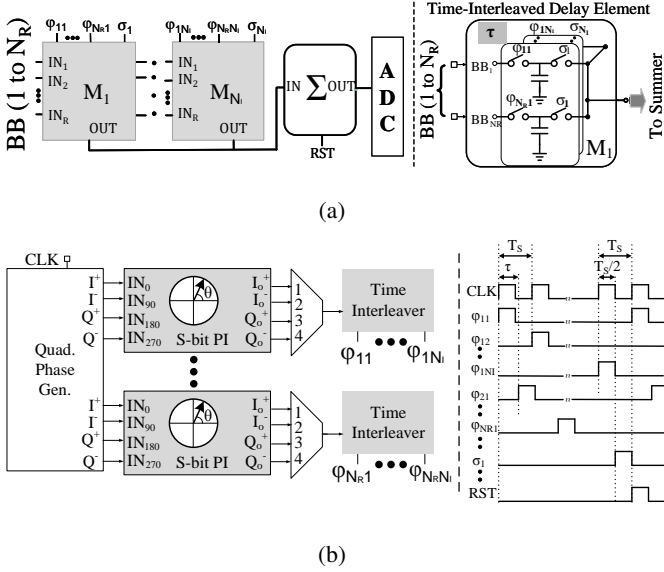


Fig. 6. (a) Multiply-and-accumulate in discrete-time for TTD BF [22], [25] (inset: switched-capacitor adder without the opamp) and (b) time-interleaved clock generation unit (inset: example timing diagram).

applications, including the spectral efficiency in mmW data communication and position error in localization.

#### IV. ARCHITECTURE PERFORMANCE ANALYSIS

In this section, we introduce and compare the baseband implementation of analog TTD elements in analog and hybrid TTD architectures. Then we study the impact of limited TTD delay range in both architectures on beam training performance and we explain the interplay between the number of antenna elements  $N_R$ , bandwidth BW, and diversity order  $R$ . We also numerically evaluate the impact of hardware impairments and ADC quantization error on the AoA estimation accuracy.

##### A. Baseband Implementation of Analog TTD Front-End

While TTD array operation is conceptually simple, its physical implementation is non-trivial when targeting large delay range. In general, implementing delays with large range-to-resolution ratios is difficult without severe penalties in linearity, noise, power and area besides increased design complexity. In an array with baseband TTD elements, instead of delaying the down-converted and phase shifted signals from the antennas, sampling and digitization, the signals are sampled at different time instants through the Switched-Capacitor Arrays (SCA) circuit, resulting in the same digitized value. Thus, the complexity of delaying signals is shifted to the clock path where precise and calibrated delays can be applied in the advanced semiconductor technology nodes. More importantly, a large delay range-to-resolution ratio can be realized easily. The SCA based implementation requires multiple time-interleaved and delay-compensated phases for formation of the beam as shown in Fig. 6(a) and discussed in detail in [22]. In the sampling phase, the input signal from each channel is first sampled (with delayed clocks) on a sampling capacitor ( $C_S$ ). After the last sampling phase, the stored charges on

TABLE II  
ANALOG TTD ARRAY COMPLEXITY WITH INCREASED DIVERSITY  $R$ .

$R$	$\Delta\tau$	$\tau_{A,N_R}$ Analog	$N_I$ Analog	$\tau_{A,N_R}$ Hybrid	$N_I$ Hybrid
1	0.5 ns	7.5 ns	31	1.5 ns	7
2	1 ns	15 ns	61	3 ns	13
4	2 ns	30 ns	121	6 ns	25

Assumed parameters are  $N_R = 16$ ,  $f_{CLK} = 4$  GHz,  $BW = 2$  GHz. Hybrid TTD array has four 4-element sub-arrays ( $N_I=4$ ).

each capacitor corresponding to each channel (and each time-interleaved phase) are summed to form the beam.

The proposed beam-training algorithm requires wider delay ranges with delay offsets that are integer multiples of  $\Delta\tau$ . This significantly relaxes the design requirement of the SCA and the clock path for TTD-based beam-training. Larger delay-bandwidth products can thus be realized using passive SCA whose performance will not be limited by the opamp feedback factor or time-based circuits as demonstrated in our recent work in [23]. Ongoing research is also investigating use of high-linearity and high-speed ring amplifiers [26] in the SCA.

Fig. 6(b) shows the clock generation circuit. The proposed beam-training just requires a time-interleaver applied to the input clock. The output of the time-interleaver is applied to interleaved multiply-and-accumulate units (MAC) in the SCA ( $=N_I$ ) and enables the SCA to span the required delay range while meeting the Nyquist BW. The same circuit can be extended for data communication with the only addition being a multi-bit phase interpolator (PI) as described in [25]. In Fig. 6(b), the external single-phase clock (CLK) is first fed to a quadrature phase generator circuit. The quadrature outputs ( $I^-$ ,  $I^+$ ,  $Q^-$ ,  $Q^+$ ) of each phase generator are further fed to the S-bit PI. The quadrature output is then applied to a multiplexer (MUX) which helps in spanning the angular range ( $-\pi/2, \pi/2$ ). An example timing diagram is also shown in Fig. 6(b) with  $N_R = 4$  and  $N_I = 7$  for  $R = 1$  in a hybrid array. A total of 36 phases are shown at the time-interleaver output with a 12.5% pulse width.

We further analyze the number of interleaving levels that are required in analog and hybrid TTD arrays. Considering  $N_I$  as the interleaving factor in the analog TTD array (Fig. 1), the maximum achievable delay compensation  $T_{C-max}$  is

$$T_{C-max} = (N_I - 1)T_s = (N_I - 1)/f_s \quad (14)$$

where  $T_s$  and  $f_s$  are the reference clock period and sampling frequency respectively. To cover the entire angular range in beam training,  $T_{C-max}$  should be equal to  $\tau_{A,N_R}$ . Substituting (6) in this equality and solving for  $T_s$  yields

$$T_s = (N_R - 1)R / ((N_I - 1)BW) \quad (15)$$

Considering a heterodyne receiver architecture and perfect sampled signal reconstruction satisfying the Nyquist condition (i.e.,  $T_s \leq 1/(2BW)$ ),  $N_I$  can be derived to be

$$N_I \geq 1 + 2R(N_R - 1). \quad (16)$$

Equation (16) can be further applied for hybrid arrays substituting  $N_R$  with  $N_R/N_H$ .

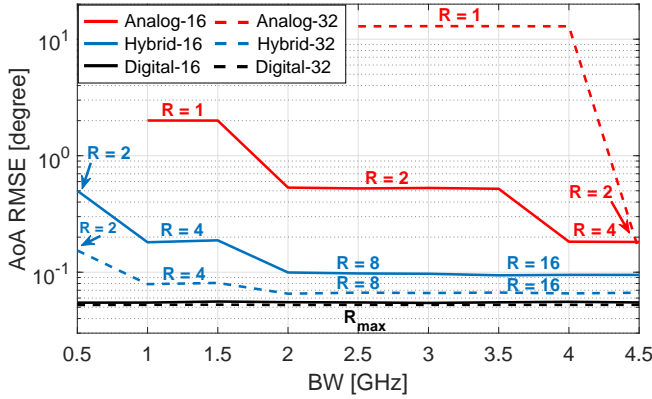


Fig. 7. Beam training performance comparison of the three considered architectures and the interplay of  $R$ ,  $N_R$ , and BW.

Table II shows an example case study of the required number of interleaving stages in the analog/hybrid TTD array as a function of diversity order and the delay range. This table uses (16) with a specific case of 2 GHz bandwidth, 4 GHz sampling frequency, and 16 antenna elements for both the analog and hybrid array presented in Fig. 1 and Fig. 2 respectively.

### B. Impact of Limited TTD Delay Range on Beam Training

In this subsection, we assume that the analog and hybrid architectures have TTD elements with the same state-of-the-art maximum delay compensation of  $T_{C-\max} = 15$  ns, or equivalently the same interleaving factor  $N_I$ .

To realize the proposed beam training algorithm,  $\tau_{A,N_R} \leq T_{C-\max}$  needs to be satisfied for the analog, and  $\tau_{A,N_I} \leq T_{C-\max}$  for the hybrid TTD array. Based on these conditions, it is straightforward to show that the achievable diversity order  $R$  is limited as

$$1 \leq R \leq \frac{T_{C-\max}}{N_R - 1} BW \quad \text{and} \quad 1 \leq R \leq \frac{T_{C-\max}}{N_I - 1} BW, \quad (17)$$

for the analog and hybrid array, respectively. Note that with  $R < 1$ , the beam training algorithm cannot be realized with a single OFDM symbol. The expressions in (17) describe the dependency of  $R$  on the basic system parameters  $N_R$ ,  $N_I$ , and BW. In the remainder of this subsection, we numerically evaluate the interplay among them.

We study the beam training performance of different architectures in terms of AoA estimation accuracy, assuming that  $R$  is constrained to be maximal power of 2. We consider a system with carrier frequency  $f_c = 60$  GHz, bandwidth values in the range  $0.5 \text{ GHz} \leq BW \leq 4.5 \text{ GHz}$ , and  $M_{\text{tot}} = 4096$  subcarriers for any bandwidth. The transmitter array size is  $N_T = 128$ , while the receive array size can take values  $N_R = \{16, 32\}$ . There are  $N_I = 4$  antennas in each sub-array in hybrid TTD architecture, regardless of the total number of antennas. The number of probed directions in beam training is assumed to be  $D = 2N_R$  and the dictionary size is  $Q = 1024$ . The channel consists of  $L = 3$  clusters, where one is 10 dB stronger than the other two. Fading is simulated by 20 rays within each cluster with up to 10 ns spread. There is no intra-cluster angular spread. Pre-beamforming signal-to-noise ratio

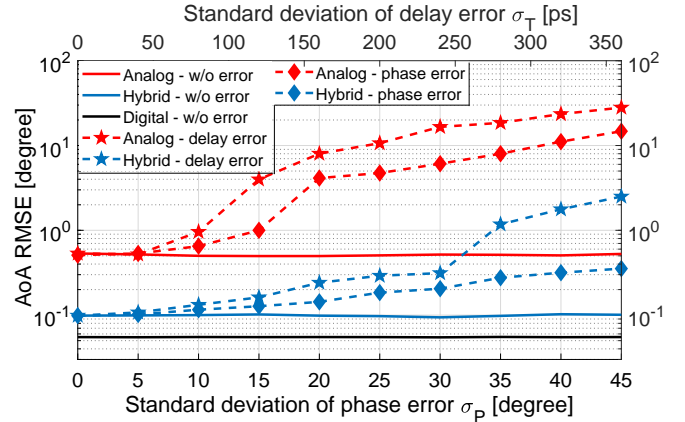


Fig. 8. Beam training performance comparison of the three considered architectures under the distorted delay taps  $\tilde{\tau}_n \sim \mathcal{N}(\tau_n, \sigma_\tau^2)$ ,  $\forall n$ , and phase taps  $\tilde{\phi}_n \sim \mathcal{N}(\phi_n, \sigma_\phi^2)$ ,  $\forall n$ . The curves with the delay error (dashed with stars) and phase error (dashed with diamonds) are associated with the upper and lower x-axis, respectively.

(SNR) is defined as  $\text{SNR} \triangleq \sum_{l=1}^L \sigma_l^2 / \sigma_N^2$ , and it is assume to be  $\text{SNR} = -20$  dB.

In Fig. 7, we present the results for the beam training performance and the interplay of the considered parameters. In both cases  $N_R = 16$  and  $N_R = 32$ , the analog TTD array architecture has the highest RMSE of AoA estimation due to low achievable diversity order  $R$ . As discussed earlier, analog arrays have large delay range requirements, and thus better estimation accuracy (equivalently, higher  $R$ ) requires larger BW. Similarly, increasing the array size  $N_R$  can have a positive effect on the performance. However, if BW is not large enough and there is no diversity ( $R = 1$ ), larger arrays do not improve the estimation accuracy in frequency-selective channels. The analog arrays do not have the results for the values of BW for which the proposed single-shot beam training cannot be realized ( $R < 1$ ). In hybrid TTD arrays, higher diversity orders can be utilized since  $N_I < N_R$ , which leads to better estimation accuracy compared to analog arrays. Increase in the number of antenna elements does not change achievable  $R$  in hybrid arrays since we assume that  $N_I = 4$  remains constant. It does, however, improve the estimation accuracy of hybrid arrays, which approaches the sub-degree performance of fully digital arrays. Since  $R$  can be maximized through DSP in digital arrays, their performance is independent of BW. The floor of the AoA RMSE is determined by the dictionary size  $Q = 1024$ . Based on described results in Fig. 7, one can predict the diversity order  $R$  and beam training performance for any considered array architecture, given the system parameters BW,  $N_R$ , and  $T_{C-\max}$ .

### C. Impact of TTD Hardware Impairments on Beam Training

Next, we study the impact of practical TTD hardware impairments and ADC quantization errors on beam training in all considered architectures. Here we keep AoA RMSE as the performance metric and use the same system parameters as in the previous subsection. We consider a specific case with  $N_R = 16$  and  $BW = 2$  GHz.

In Fig. 8, we study the beam training performance under the phase and delay errors. Unlike analog and hybrid TTD arrays,

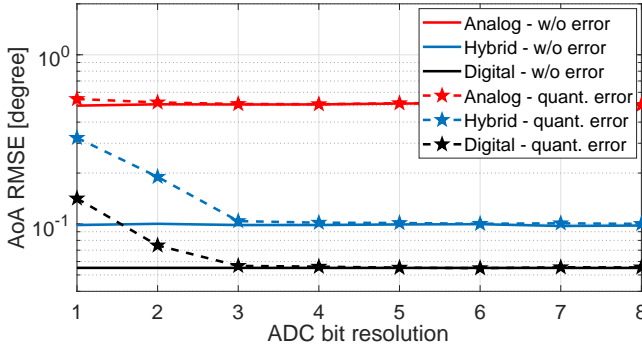


Fig. 9. Beam training performance comparison of the three considered architectures under different ADC resolutions.

fully digital array is not sensitive to these hardware impairments and we include its performance with the maximum  $R$  as the benchmark. With the considered system parameters, analog TTD array has the diversity order  $R = 2$ , which limits its angle estimation accuracy and robustness to hardware errors. We can see that the beam training algorithm can tolerate phase errors with the standard deviation of up to  $\sigma_P = 15^\circ$  and delay errors with the standard deviation of up to  $\sigma_T = 75$  ps. Hybrid TTD array achieves a lower estimation accuracy and greater robustness to delay and phase errors than analog TTD array since it leverages the diversity order  $R = 8$  in beam training. It can tolerate large phase errors and delay errors with the standard deviation larger than  $\sigma_T = 200$  ps. It is worth noting that the delay errors in hybrid arrays are independent of the reduced delay taps in the corresponding TTD elements.

In Fig. 9, we present how finite ADC resolution affects the beam training performance with different array architectures. For fair comparison, we assume that the automatic gain control (AGC) outputs a unit-variance signal in all architectures. We can observe that the AoA estimation accuracy of the analog TTD array with a single RF-chain is marginally affected by low ADC resolution. On the other hand, low resolution ADCs have a noticeable impact on beam training with the hybrid TTD and fully digital arrays, as combined quantization errors from different RF-chains deteriorate the estimation accuracy. We note, however, that the deteriorated accuracy is still within the sub-degree range and lower than that of the analog array. Our results indicate that practical mmW and sub-THz transceivers may require ADCs with only a few bits of resolution for effective beam training. For example, with only 3-bit resolution, the performance loss is negligible in any array. Low-resolution ADCs have a positive impact on the overall power efficiency of the considered TTD architectures, as discussed in the next section.

## V. POWER ANALYSIS OF TTD ARCHITECTURES

This section presents power analysis of the analog and hybrid TTD arrays comparing it with a digital array for the proposed mmW beam training algorithm in Section III-B. We will estimate the power consumption of the baseband components in the signal chain in Fig. 1, Fig. 2, and Fig. 3 for the analog, hybrid, and digital arrays assuming the mmW front-end consumes the same power in all the three array

TABLE III  
STATE-OF-THE-ART LOW-RESOLUTION GHZ ADCs.

Parameters	[28]	[29]	[30]
Sampling Rate ( $f_s$ )(MHz)	2500	2000	5
ENOB (bit)	6	7.93	4.06
Power ( $\mu$ W)	7500	21000	78000
FoM (fJ/c-s)	74.7	119	94.6
Technology (nm)	65	65	65

architectures. The only exception to this assumption in the front-ends of the three array architectures is the phase-shifter. In the analog/hybrid TTD array, the phase shifter precedes the downconverting mixer whereas for the digital array it can be implemented after the ADC. For the sake of comparison in this work, we consider the digital phase-shifter power equivalent to that of the RF/LO phase-shifter which will be assumed to have a complete passive implementation [27]. The estimation methodology for the remaining components of the hybrid and the digital arrays follows that of the analog TTD array as described in the next subsections. For each component, we also have provided an example based on Table II.

### A. Power Consumption of Analog/Hybrid TTD Array

Referring Fig. 1 (Fig. 2), this subsection will estimate the power consumption of the ADC, AGC, SCA, and the time-interleaving blocks that differentiates the power consumption in the analog (hybrid) arrays.

1) *Analog-to-Digital Converter (ADC)*: We estimate the ADC power consumption using figure-of-Merit (FoM) derived from recent works [28]–[30] on low-resolution high-speed flash ADCs (different ADC configuration can be selected when considering efficiency). Using the FoM of the state-of-the-art flash ADCs from Table III, we take the average FoM of 96.1fJ/c-s for our estimation. For a 3-bit ENOB,  $f_s=4$ GHz and a FoM of 96.1fJ/c-s, the estimated power is thus 3.07mW.

In addition to the ADC power consumption, we also estimate the deserializer power that is needed to interface the high-speed ADCs with the backend DSP. Though insignificant for analog and hybrid arrays, it will be an important contributor for digital arrays. We consider here the DSP operating at 1GHz and estimate the deserializer power consumption. From [31], excluding the power of clock generator, the scaled deserializer power for one unit ( $P_{DES0}$ ) is found to be 0.512 mW ( $= 3.2 \times 4/25$ ) which yields 1.5mW and 6mW of power consumption in analog and hybrid array respectively.

2) *Switched-Capacitor Array (SCA)*: The SCA power consumption is dominated mostly by the feedback operational transconductance amplifier (OTA). We estimate the OTA power consumption for an analog array similar to the method in [22]. The DC gain ( $A_0$ ) and the unity-gain bandwidth ( $\omega_u$ ) requirements of the OTA used in the SCA are found to be:

$$\omega_u = 2 \ln(2) N_R (x + 1) f_s$$

where  $x$  is the ADC resolution and  $f_s$  is the ADC sampling frequency.

The normalized unity-gain bandwidth ( $\omega_{u0}$ ) per unit sampling frequency can be written as:  $\omega_{u0} = 2 \ln(2)(x + 1)$ .



For a 3-bit ADC (referring Fig. 9), the normalized unity-gain frequency  $\omega_{u0} = 2\ln(2)(3 + 1) = 5.54$  Hz. Neglecting parasitics, second order effects, and considering a two-stage internally compensated OTA, the transconductance of this OTA can be designed to be linearly dependent to the DC current. As a result, the DC gain of the OTA is independent of its DC current and power consumption  $P_{OTA}$ . At the same time,  $\omega_u$  is a linear function of the OTA transconductance, and thus varies proportionally to  $P_{OTA}$ . Given these assumptions, the minimum requirement on the OTA  $\omega_u$  results in linear dependency of  $P_{OTA}$  to the product of the number of antennas and sampling frequency, as shown below [22]:

$$P_{OTA} \approx P_{OTA0} N_R f_s$$

where  $P_{OTA0}$  is the power consumption of an OTA designed for a single-element array with unit sampling frequency (1Hz). Solving for a  $60^\circ$  phase margin (PM) requirement puts  $C_c$  close to 0.22 pF yielding  $g_{mn} = 0.22 \text{ pF} \times 5.54 = 1.2188 \text{ ps}$ . Assuming  $g_m/I_D = 15$ , the unit current can be obtained as  $I_{Dn} = 8.1253 \times 10^{-14} \text{ A}$ . For a  $60^\circ$  PM, the  $g_{mn}$  for the second stage is around 10 times of the first stage and we further assume the same  $g_m/I_D$  ratio. The total current is thus  $(2 + 10)I_{Dn} = 9.7504 \times 10^{-13} \text{ A}$ . Assume a 1V supply, the  $P_{OTA0}$  can be estimated as  $9.7504 \times 10^{-13} \text{ W}$ . For the 16-antenna array and  $f_s = 4\text{GHz}$  (Table II), the estimated power consumption is thus 62.403 mW. Note that the hybrid TTD array relaxes the OTA power consumption per sub-array where  $P_{OTA}$  is scaled by  $N_R/N_H$ . The same power consumption estimation however applies to a digital array without any relaxation.

The power consumption of the AGC can also be estimated using,  $P_{AGC}$ . Assuming  $P_{AGC}$  consumes the same power as the OTA, the estimated total  $P_{AGC}$  is also equal to 3.9mW for analog arrays and 15.6mW for the hybrid array following the design specifications in Table II.

3) *Time-Interleaver*: The power consumption for the time interleaver can be estimated as [32]:

$$P_{TINW} = f_s/N_I \times N_I \times (C_{sw}/N_I + C_{int}) \times VDD^2$$

where  $C_{sw}$  is the switch capacitance and  $C_{int}$  is the interconnect parasitic capacitance. For a sampling frequency of 4GHz and 1V supply,  $C_{sw} = 2.5\text{pF}$ ,  $C_{int} = 0.6\text{pF}$  [32], 31 levels of time interleaving in analog array, and 7 levels of interleaving in a hybrid array, the estimated power consumption of the time interleaver is 2.7mW and 3.8mW for the analog and digital hybrid arrays respectively.

### B. Power Consumption of Digital Array

The estimated power consumption for digital TTD array can be derived following a similar approach to the analog arrays with the important consideration that the proposed beam training algorithm will require only integer delays at the ADC sampling frequency. For operation in communication mode, fractional-rate samplers will be needed as detailed in [33]. In addition to the same number of ADCs, AGCs and filters as in an analog TTD array, the digital array consumes higher power

TABLE IV  
POWER ESTIMATION METHODOLOGY FOR TTD ARRAYS.

# Components	Analog	Hybrid	Digital
ADC	1	$N_H$	$N_R$
SCA/AGC	1	$N_H$	$N_R$
$P_{SCA}$	$P_{OTA0} N_R f_s$	$P_{OTA0} N_R / N_H f_s$	$P_{OTA0} N_R f_s$
$P_{ADC, x\text{-bit}}$	FoM based estimation		
$P_{AGC}$	$P_{OTA0} f_s$	$P_{OTA0} N_H f_s$	$P_{OTA0} N_R f_s$
$P_{DeSer}$	$P_{DES0} f_s x$	$P_{DES0} N_H x$	$P_{DES0} N_R x$

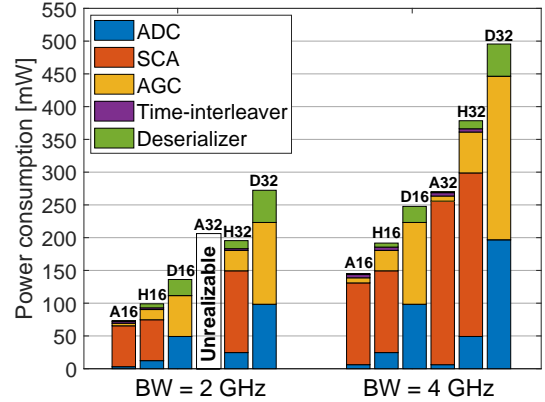


Fig. 10. Comparison of analog (A), hybrid (H), and digital (D) architectures in terms of power consumption for  $N_R = \{16, 32\}$  and  $BW = \{2, 4\}\text{GHz}$ .

at the ADC-DSP interface primarily due to the need for deserializing the high-speed ADC output. For example, with 16-elements and 3-bit per ADC, the estimated power consumption of the deserializer will be 24.6mW.

### C. Comparison of Estimated Array Power Consumption

Table IV summarizes the required number of components and power consumption in the analog, hybrid, and digital arrays based on the architectures in Fig. 1, Fig. 2, and Fig. 3, respectively. Fig. 10 illustrates the introduced power estimation methodology with a breakdown of individual components for the analog and hybrid TTD arrays and also the benchmark digital array. The estimated power consumption for each component block is described in the previous subsections for each array architecture. The analog array provides high energy efficiency as compared to the hybrid TTD array and digital arrays. However, the increasing bandwidth as well as the number of elements requires larger unity-gain bandwidths OTAs which increases design complexity for higher diversity orders. The need for higher unity-gain bandwidths is further constrained with increasing number of feedback to the virtual ground of the OTA. Hybrid arrays are thus the most optimal choice to meet feasible delay-bandwidth products. Future work will investigate design of analog (hybrid) arrays with higher number of antenna elements per sub-array using passive SCA that leverages the reasonably lower resolutions ( $\approx 3$ -bit) required by the proposed beam training algorithm.

## VI. CONCLUSIONS AND FUTURE WORK

This work introduced and analyzed two TTD architectures with large delay-bandwidth product baseband delay elements

as potential candidates for mmW beam training. We demonstrated that a high AoA estimation accuracy can be achieved with both proposed TTD architectures using a power measurement based beam training scheme, which requires only one wideband training pilot. The dependency of the codebook design and beam training performance on system parameters, including the bandwidth, number of antenna elements, and maximum TTD delay compensation, was analyzed and numerically evaluated in a practical multipath fading channel. Detailed analysis of the angle estimation accuracy, robustness to hardware impairments, and power consumption, revealed the trade-offs between the proposed TTD architectures when benchmarked against the digital array. The analog TTD array consumes 66% less power than the digital array, but it achieves a higher angle estimation error. The hybrid TTD array has a comparable beam training performance and 25% lower power consumption than the digital array. The results on how power consumption scales with the key system parameters, including the bandwidth and array size, provided an insight into the beam training design for future mmW and sub-THz systems. Future work will include array implementations supporting larger delay-bandwidth products for arrays with higher number of antenna elements, as well as channel estimation and identification of multiple AoAs in interference-limited networks.

#### APPENDIX A

##### DERIVATION OF EXPECTED POWERS IN $D$ DIRECTIONS

We consider a frequency-selective multipath channel with  $L$  clusters and corresponding gains modeled as  $G_l \sim \mathcal{CN}(0, \sigma_l^2)$ . The channel gains are assumed to be independent over different clusters and frequency sub-bands. The frequency domain channel model can be approximated as

$$\mathbf{H} = \mathbf{A}_R \mathbf{\Lambda} \mathbf{A}_T^H, \quad (18)$$

where  $\mathbf{A}_R \in \mathbb{C}^{N_R \times Q}$  and  $\mathbf{A}_T \in \mathbb{C}^{N_T \times Q}$  contain  $Q$  array responses  $\mathbf{a}_R(\xi_q)$  and  $\mathbf{a}_T(\xi_q)$  that correspond to  $Q$  uniformly spaced angles  $\xi_q$ ,  $q = 1, \dots, Q$ , in the range  $(-\pi/2, \pi/2)$ . The elements of array responses are defined as  $[\mathbf{a}_R(\theta)]_n = N_R^{-1/2} \exp(-j(n-1)\pi \sin(\theta))$ ,  $n = 1, \dots, N_R$ , and  $[\mathbf{a}_T(\theta)]_n = N_T^{-1/2} \exp(-j(n-1)\pi \sin(\theta))$ ,  $n = 1, \dots, N_T$ . The square matrix  $\mathbf{\Lambda} \in \mathbb{C}^{Q \times Q}$  has only  $L$  non-zero elements that correspond to the gains  $G_l$ ,  $\forall l$ . Commonly,  $Q \gg L$  and the approximation error in (18) can be neglected.

With the codebook design described in Section III-B, the received signal in any sounded direction  $d$  can be considered as a zero-mean complex Gaussian random variable and expressed as

$$Y_d = \mathbf{f}_d^H \mathbf{H} \mathbf{v} + \mathbf{f}_d^H \mathbf{n}, \quad (19)$$

where  $\mathbf{n} \sim \mathcal{CN}(0, \sigma_{\mathbf{N}}^2 \mathbf{I}_R)$  is white Gaussian noise. The realizations of (19) are received symbols  $Y[m]$ ,  $m \in \mathcal{M}_d$ . The expected received signal power in direction  $d$  is  $p_d = \mathbb{E}[|Y_d|^2] = \mathbb{E}[(\mathbf{f}_d^H \mathbf{H} \mathbf{v} M^{-1/2} + \mathbf{f}_d^H \mathbf{n})^H (\mathbf{f}_d^H \mathbf{H} \mathbf{v} M^{-1/2} + \mathbf{f}_d^H \mathbf{n})]$ . Based on the channel model in (18), it can be shown that

$$p_d = M^{-1} \mathbb{E}[\mathbf{v}^H \mathbf{A}_T \mathbf{\Lambda}^* \mathbf{A}_R^H \mathbf{f}_d \mathbf{f}_d^H \mathbf{A}_R \mathbf{\Lambda} \mathbf{A}_T^H \mathbf{v}] + \mathbb{E}[\mathbf{n}^H \mathbf{f}_d \mathbf{f}_d^H \mathbf{n}]. \quad (20)$$

We apply the trace operator  $\text{Tr}(\cdot)$  to (20) and exploit its linearity and cyclic property to obtain

$$\begin{aligned} p_d &= M^{-1} \mathbb{E}[\text{Tr}(\mathbf{\Lambda} \mathbf{A}_T^H \mathbf{v} \mathbf{v}^H \mathbf{A}_T \mathbf{\Lambda}^* \mathbf{A}_R^H \mathbf{f}_d \mathbf{f}_d^H \mathbf{A}_R)] + N_R \sigma_{\mathbf{N}}^2 \\ &= \text{Tr}(\mathbf{G} \mathbf{A}_R^H \mathbf{f}_d \mathbf{f}_d^H \mathbf{A}_R) + N_R \sigma_{\mathbf{N}}^2. \end{aligned} \quad (21)$$

where  $\mathbf{G} = \mathbb{E}[\mathbf{\Lambda} \mathbf{A}_T^H \mathbf{v} \mathbf{v}^H \mathbf{A}_T \mathbf{\Lambda}^*]$ . Since  $\mathbf{\Lambda}$  and  $\mathbf{\Lambda}^*$  are sparse matrices,  $[\mathbf{\Lambda} \mathbf{A}_T^H \mathbf{v} \mathbf{v}^H \mathbf{A}_T \mathbf{\Lambda}^*]$  yields another sparse  $Q \times Q$  matrix with  $L^2$  non-zero elements. There are  $L$  non-zero elements of the form  $|G_l|^2 |\mathbf{a}_T^H(\theta_l^{(T)}) \mathbf{v}|^2$ ,  $\forall l$ , on the main diagonal. The  $L(L-1)$  off-diagonal elements are cross terms  $G_{l_1} G_{l_2}^* \mathbf{a}_T^H(\theta_{l_1}^{(T)}) \mathbf{v} \mathbf{v}^H \mathbf{a}_T(\theta_{l_2}^{(T)})$ ,  $\forall l_1, l_2$ . Thus,  $\mathbf{G}$  is a diagonal matrix with  $L$  non-zero elements  $\sigma_l^2 |\mathbf{a}_T^H(\theta_l^{(T)}) \mathbf{v}|^2$ ,  $\forall l$ , since  $\mathbb{E}[G_{l_1} G_{l_2}^*] = 0$ ,  $\forall l_1 \neq l_2$ , and  $\mathbb{E}[|G_l|^2] = \sigma_l^2$ ,  $\forall l$ . The product of  $\mathbf{G}$  and the matrix of the UE BF gains  $\mathbf{A}_R^H \mathbf{f}_d \mathbf{f}_d^H \mathbf{A}_R$  is a  $Q \times Q$  matrix whose diagonal elements are equal to  $|\mathbf{f}_d^H \mathbf{a}_R(\xi_q)|^2 [\mathbf{G}]_{q,q}$ , so (21) becomes

$$p_d = \mathbf{b}_d^T \mathbf{g} + N_R \sigma_{\mathbf{N}}^2 \quad (22)$$

where  $\mathbf{b}_d = [|\mathbf{f}_d^H \mathbf{a}_R(\xi_1)|^2, |\mathbf{f}_d^H \mathbf{a}_R(\xi_2)|^2, \dots, |\mathbf{f}_d^H \mathbf{a}_R(\xi_Q)|^2]^T$  and  $\mathbf{g} = \text{diag}(\mathbf{G})$ . By vectorizing the result in (22), we obtain

$$\mathbf{p} = \mathbf{B} \mathbf{g} + N_R \sigma_{\mathbf{N}}^2 \mathbf{1}, \quad (23)$$

where  $\mathbf{p} = [p_1, p_2, \dots, p_D]^T$  and  $\mathbf{B} = [\mathbf{b}_1, \mathbf{b}_2, \dots, \mathbf{b}_D]^T$ . Since the BS provides a large BF gain with the fixed precoder  $\mathbf{v}$ , we can assume that receiver array sees only one spatially filtered dominant cluster, e.g., the first one. Consequently, there is only one non-zero element in  $\mathbf{g}$  equal to  $|\mathbf{a}_T^H(\theta_1^{(T)}) \mathbf{v}|^2 \sigma_1^2$ .

#### REFERENCES

- [1] J. G. Andrews, S. Buzzi, W. Choi, S. V. Hanly, A. Lozano, A. C. K. Soong, and J. C. Zhang, "What will 5G be?" *IEEE Journal on Selected Areas in Communications*, vol. 32, no. 6, pp. 1065–1082, June 2014.
- [2] T. S. Rappaport, Y. Xing, G. R. MacCartney, A. F. Molisch, E. Mellios, and J. Zhang, "Overview of millimeter wave communications for fifth-generation (5G) wireless networks with a focus on propagation models," *IEEE Transactions on Antennas and Propagation*, vol. 65, no. 12, pp. 6213–6230, 2017.
- [3] K. Witrals, P. Meissner, E. Leitinger, Y. Shen, C. Gustafson, F. Tufveson, K. Haneda, D. Dardari, A. F. Molisch, A. Conti, and M. Z. Win, "High-accuracy localization for assisted living: 5G systems will turn multipath channels from foe to friend," *IEEE Signal Processing Magazine*, vol. 33, no. 2, pp. 59–70, 2016.
- [4] K. Hosoya, N. Prasad, K. Ramchandran, N. Orihashi, S. Kishimoto, S. Rangarajan, and K. Maruhashi, "Multiple sector ID capture (MIDC): A novel beamforming technique for 60-GHz band multi-Gbps WLAN/PAN systems," *IEEE Transactions on Antennas and Propagation*, vol. 63, no. 1, pp. 81–96, 2015.
- [5] C. Jeong, J. Park, and H. Yu, "Random access in millimeter-wave beamforming cellular networks: issues and approaches," *IEEE Communications Magazine*, vol. 53, no. 1, pp. 180–185, 2015.
- [6] J. Kim and A. F. Molisch, "Fast millimeter-wave beam training with receive beamforming," *Journal of Communications and Networks*, vol. 16, no. 5, pp. 512–522, 2014.
- [7] L. Zhou and Y. Ohashi, "Efficient codebook-based MIMO beamforming for millimeter-wave WLANs," in *2012 IEEE 23rd International Symposium on Personal, Indoor and Mobile Radio Communications - (PIMRC)*, 2012, pp. 1885–1889.
- [8] D. Zhang, A. Li, H. Chen, N. Wei, M. Ding, Y. Li, and B. Vucetic, "Beam allocation for millimeter-wave MIMO tracking systems," *IEEE Transactions on Vehicular Technology*, vol. 69, no. 2, pp. 1595–1611, 2020.
- [9] H. Yan and D. Cabric, "Compressive initial access and beamforming training for millimeter-wave cellular systems," *IEEE Journal of Selected Topics in Signal Processing*, vol. 13, no. 5, pp. 1151–1166, 2019.

- [10] M. Bajor et al, "A flexible phased-array architecture for reception and rapid direction-of-arrival finding utilizing pseudo-random antenna weight modulation and compressive sampling," *IEEE J. Solid-State Circuits*, vol. 54, no. 5, pp. 1315–1328, May 2019.
- [11] A. Ali, N. Gonzalez-Prelcic, and R. W. Heath, "Millimeter wave beam-selection using out-of-band spatial information," *IEEE Transactions on Wireless Communications*, vol. 17, no. 2, pp. 1038–1052, 2018.
- [12] V. Desai, L. Krzymien, P. Sartori, W. Xiao, A. Soong, and A. Alkhateeb, "Initial beamforming for mmWave communications," in *2014 48th Asilomar Conference on Signals, Systems and Computers*, 2014, pp. 1926–1930.
- [13] C. N. Barati, S. A. Hosseini, S. Rangan, P. Liu, T. Korakis, and S. S. Panwar, "Directional cell search for millimeter wave cellular systems," in *2014 IEEE 15th International Workshop on Signal Processing Advances in Wireless Communications (SPAWC)*, 2014, pp. 120–124.
- [14] C. N. Barati, S. A. Hosseini, M. Mezzavilla, T. Korakis, S. S. Panwar, S. Rangan, and M. Zorzi, "Initial access in millimeter wave cellular systems," *IEEE Transactions on Wireless Communications*, vol. 15, no. 12, pp. 7926–7940, 2016.
- [15] S. Kalia, S. A. Patnaik, B. Sadhu, M. Sturm, M. Elbadry, and R. Harjani, "Multi-beam spatio-spectral beamforming receiver for wideband phased arrays," *IEEE Transactions on Circuits and Systems I: Regular Papers*, vol. 60, no. 8, pp. 2018–2029, 2013.
- [16] C. Yeh, T. Chu, C. Chen, and C. Yang, "A hardware-scalable DSP architecture for beam selection in mm-Wave MU-MIMO systems," *IEEE Transactions on Circuits and Systems I: Regular Papers*, vol. 65, no. 11, pp. 3918–3928, 2018.
- [17] S. Blandino, G. Mangraviti, C. Desset, A. Bourdoux, P. Wambacq, and S. Pollin, "Multi-user hybrid MIMO at 60 GHz using 16-antenna transmitters," *IEEE Transactions on Circuits and Systems I: Regular Papers*, vol. 66, no. 2, pp. 848–858, 2019.
- [18] N. J. Karl, R. W. McKinney, Y. Monnai, R. Mendis, and D. M. Mittleman, "Frequency-division multiplexing in the terahertz range using a leaky-wave antenna," *Nature Photonics*, vol. 9, no. 11, p. 717, 2015.
- [19] Y. Ghasempour, C.-Y. Yeh, R. Shrestha, D. Mittleman, and E. Knightly, "Single shot single antenna path discovery in THz networks," in *Proceedings of the 26th Annual International Conference on Mobile Computing and Networking*, ser. MobiCom 20. New York, NY, USA: Association for Computing Machinery, 2020. [Online]. Available: <https://doi.org/10.1145/3372224.3380895>
- [20] H. Yan, V. Boljanovic, and D. Cabric, "Wideband millimeter-wave beam training with true-time-delay array architecture," in *2019 53rd Asilomar Conference on Signals, Systems, and Computers*, 2019, pp. 1447–1452.
- [21] T. Chu and H. Hashemi, "A true time-delay-based bandpass multi-beam array at mm-waves supporting instantaneously wide bandwidths," in *2010 IEEE International Solid-State Circuits Conference - (ISSCC)*, 2010, pp. 38–39.
- [22] E. Ghaderi, A. Sivadhasan Ramani, A. A. Rahimi, D. Heo, S. Shekhar, and S. Gupta, "An integrated discrete-time delay-compensating technique for large-array beamformers," *IEEE Trans. Circuits Syst. I*, vol. 66, no. 9, pp. 3296–3306, Sep. 2019.
- [23] E. Ghaderi, C. Puglisi, S. Bansal, and S. Gupta, "10.8 A 4-element 500MHz-modulated-BW 40mW 6b 1GS/s analog-time-to-digital-converter-enabled spatial signal processor in 65nm CMOS," in *2020 IEEE International Solid-State Circuits Conference (ISSCC)*, Feb. 2020.
- [24] V. Boljanovic, H. Yan, E. Ghaderi, D. Heo, S. Gupta, and D. Cabric, "Design of millimeter-wave single-shot beam training for true-time-delay array," *arXiv.org*, 2020. [Online]. Available: <https://arxiv.org/abs/2002.07849>
- [25] E. Ghaderi, A. Sivadhasan Ramani, A. A. Rahimi, D. Heo, S. Shekhar, and S. Gupta, "A 4-channel MIMO baseband receiver array with >35dB 80 MHz wideband spatial cancellation through true-time-delay and truncated Hadamard transform," *accepted for publication at IEEE Transactions on Microwave Theory and Techniques*, pp. 1–11, 2020.
- [26] B. Hershberg, S. Weaver, K. Sobue, S. Takeuchi, K. Hamashita, and U. Moon, "Ring amplifiers for switched capacitor circuits," *IEEE Journal of Solid-State Circuits*, vol. 47, no. 12, pp. 2928–2942, Dec 2012.
- [27] M. Elkholy, S. Shakib, J. Dunworth, V. Aparin, and K. Entesari, "Low-loss highly linear integrated passive phase shifters for 5G front ends on bulk CMOS," *IEEE Transactions on Microwave Theory and Techniques*, vol. 66, no. 10, pp. 4563–4575, 2018.
- [28] D. Oh, J. Kim, D. Jo, W. Kim, D. Chang, and S. Ryu, "A 65-nm CMOS 6-bit 2.5-GS/s 7.5-mW  $8 \times$  time-domain interpolating flash ADC with sequential slope-matching offset calibration," *IEEE Journal of Solid-State Circuits*, vol. 54, no. 1, pp. 288–297, 2019.
- [29] S. Zhu, B. Wu, Y. Cai, and Y. Chiu, "A 2-GS/s 8-bit non-interleaved time-domain flash ADC based on remainder number system in 65-nm CMOS," *IEEE Journal of Solid-State Circuits*, vol. 53, no. 4, pp. 1172–1183, 2018.
- [30] C. Chan, Y. Zhu, S. Sin, U. Seng-Pan, R. P. Martins, and F. Maloberti, "A 7.8-mW 5-b 5-GS/s dual-edges-triggered time-based flash ADC," *IEEE Transactions on Circuits and Systems I: Regular Papers*, vol. 64, no. 8, pp. 1966–1976, 2017.
- [31] J. W. Jung and B. Razavi, "A 25-Gb/s 5-mW CMOS CDR/deserializer," *IEEE Journal of Solid-State Circuits*, vol. 48, no. 3, pp. 684–697, 2013.
- [32] B. Razavi, "Design considerations for interleaved ADCs," *IEEE Journal of Solid-State Circuits*, vol. 48, no. 8, pp. 1806–1817, 2013.
- [33] S. Jang, R. Lu, J. Jeong, and M. Flynn, "A 1-GHz 16-element four-beam true-time-delay digital beamformer," *IEEE Journal of Solid-State Circuits*, vol. 54, no. 5, pp. 1304–1314, May 2019.